Microscopic theory of the nematic phase in $Sr_3Ru_2O_7$

S. Raghu,[1] A. Paramekanti,[2] E A. Kim,[3] R. A. Borzi,[4,5] S. A. Grigera,[4,6] A. P. Mackenzie,[4] and S. A. Kivelson[1]
[1]*Department of Physics, Stanford University, Stanford, California 94305, USA*
[2]*Department of Physics, University of Toronto, Toronto, Ontario, Canada M5S1A7*
[3]*Department of Physics, Cornell University, Ithaca, New York 14853, USA*
[4]*Scottish Universities Physics Alliance, School of Physics and Astronomy, University of St. Andrews, North Haugh, St. Andrews KY169SS, United Kingdom*
[5]*Instituto de Investigaciones Fisicoquímicas Teóricas y Aplicadas, and Departamento de Física (UNLP), IFLP (CONICET), 1900 La Plata, Argentina*
[6]*Instituto de Física de Líquidos y Sistemas Biológicos, UNLP, La Plata 1900, Argentina*
(Received 9 February 2009; published 4 June 2009)

In an externally applied magnetic field, ultrapure crystals of the bilayer compound $Sr_3Ru_2O_7$ undergo a metamagnetic transition below a critical temperature, T^*, which varies as a function of the angle between the magnetic field H and the Ru-O planes. Moreover, T^* approaches zero when H is perpendicular to the planes. This putative "metamagnetic quantum critical point," however, is pre-empted by a nematic fluid phase with order one resistive anisotropy in the *ab* plane. In a "realistic" bilayer model with moderate strength local Coulomb interactions, the existence of a sharp divergence of the electronic density of states near a van Hove singularity of the quasi-one-dimensional bands, and the presence of spin-orbit coupling results in a mean-field phase diagram which accounts for many of these experimentally observed phenomena. Although the spin-orbit coupling is not overly strong, it destroys the otherwise near-perfect Fermi-surface nesting and hence suppresses spin-density-wave ordering.

DOI: 10.1103/PhysRevB.79.214402 PACS number(s): 74.70.Pq, 71.27.+a, 71.10.Hf

I. INTRODUCTION

The Ruddlesden-Popper series $Sr_{n+1}Ru_nO_{3n+1}$ is a family of ruthenate materials which exhibit a wide variety of electronic properties ranging from unconventional superconductivity ($n=1$) to itinerant electron ferromagnetism ($n\geq 3$) and have been the focus of intense research for over a decade.[1–3] Most materials in this class are "bad metals[4]" [the resistivity $\rho(T)\propto T$ and in excess of the Ioffe-Regel limit] at room temperature and above; yet, they obey Fermi-liquid theory at low temperatures (typically $T<50$ K). The low-energy electronic properties of these materials are determined mainly by the electrons in the Ru t_{2g} subspace consisting of the nearly degenerate d_{xz},d_{yz},d_{xy} orbitals. Therefore, in addition to the spin and charge degrees of freedom, the orbital degrees of freedom play an important role in determining the properties of these systems. Here, we focus on the bilayer ($n=2$) compound $Sr_3Ru_2O_7$ which is neither a superconductor nor a ferromagnet.

$Sr_3Ru_2O_7$ is a tetragonal material consisting of RuO_2 planes forming bilayers which are stacked and weakly coupled to one another. In crystals of high-purity and structural perfection, a metamagnetic transition,[5] i.e., a sudden and sharp rise in the magnetization with a modest increase in the applied field, is observed. While this transition is first order, the transition line terminates at a critical point (H^*,T^*), where it becomes continuous (in analogy with a liquid-vapor transition in the pressure-temperature plane). However, the critical field and temperature H^* and T^* depend on the angle, θ, between the magnetic field and the crystalline c axis, perpendicular to the RuO_2 bilayers: H^* decreases from $\sim$7.8 to $\sim$5.1 T, as θ increases from 0° to 90°, while T^* drops from $T^*(\theta=90°)=1.25$ K to $T^*\sim 0$ as $\theta\rightarrow 0$, that is, when H is perpendicular to the RuO_2 planes.[6] Thus, it was proposed that this material exhibits a type of quantum critical phenomena associated with the termination point of the first-order line of metamagnetic transitions.[7] However, experiments involving ultrapure single-crystal samples (with a residual resistivity less than 1 $\mu\Omega$ cm) have shown that instead of such a "metamagnetic quantum critical point,"[8] there is a bifurcation of the metamagnetic phase boundary, which leads to *two* first-order metamagnetic transitions at closely spaced field values $H_{c1}\approx 7.8$ T and $H_{c2}\approx 8.1$ T.[9] At intermediate fields, $H_{c1}<H<H_{c2}$, an electron nematic phase[10,11] appears, which spontaneously breaks the discrete square lattice rotational symmetry from C_4 to C_2 as inferred from the observation of resistive anisotropy in the *ab* plane.[12] The nematic phase occurs in a narrow range of fields and for a range of angles $0°\leq\theta\leq 40°$ (the green region in Fig. 1). Resistive anisotropy is also found in the blue region in Fig. 1 for $55°\leq\theta\leq 90°$ but it is not known whether this reflects the existence of a new phase.

In the present paper, we study the microscopic origins of the weak metamagnetism and the accompanying nematicity. A possible microscopic route to understanding metamagnetism in this material was proposed by Binz and Sigrist[13] in a model of a two-dimensional (2D) band on a square lattice whose Fermi surface lies close to a van Hove (vH) singularity. Incorporating weak local Coulomb repulsion between the electrons, they showed that when the magnetic field tunes the Fermi surface of one spin species close enough to the vH singularity, there is a jump in magnetization. Grigera *et al.*[14] were the first to propose that the existence of the vH singularities might be a driver for nematicity accompanying metamagnetism in a spin-dependent version of the Pomeranchuk distortion[15] previously studied in the two-dimensional Hubbard and t-J models.[16,17] A critical insight into the problem of

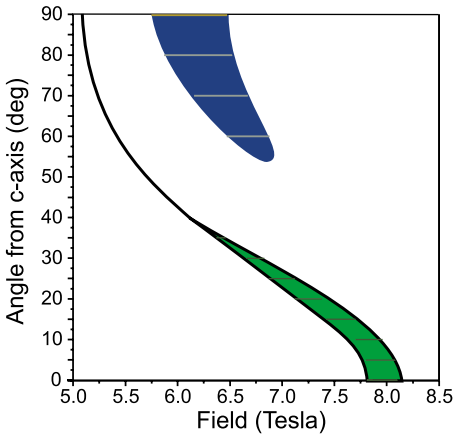

FIG. 1. (Color online) The experimentally determined low-temperature phase diagram of $Sr_3Ru_2O_7$ in the field-angle plane based on resistivity and magnetic-susceptibility measurements on shape-unbiased octagonal crystals at 100 mK. For the resistivity measurements, both the in-plane field component and the current are along either the crystallographic *a* or *b* axis. The shaded regions are those in which a resistive anisotropy is observed. The solid black lines represent first-order phase transitions as determined by a sharp dissipative peak in a measurement of the imaginary component of the ac susceptibility [see discussion in Grigera *et al.* (Ref. 6)]. We observed no dissipative peak at the boundaries of the blue region (i.e. for $55° \leqslant \theta \leqslant 90°$) but we cannot rule out its existence beyond our resolution.

nematicity accompanying metamagnetism was proposed in a paper by Kee and Kim,[18] who showed that additional interactions between the electrons can lead to new instabilities which split the metamagnetic transition, leading to an intermediate phase. Specifically, they considered a model with weak quadrupolar interactions and showed that a mean-field treatment naturally leads to a sequence of two transitions as a function of increasing H. First, at a critical field H_{c1}, the spin-up Fermi surface reconnects across the vH point at one edge of the Brillouin zone, leading to a metamagnetic jump accompanied by the spontaneous breakdown of C_4 symmetry (depending on which vH point reconnects). Then, at a higher field H_{c2}, the spin-up Fermi surface reconnects across the second vH point, leading to a second metamagnetic jump and a restoration of C_4 symmetry.

The model originally considered by Kee and Kim[18] is a single band model, with strongly $\vec{k}$-dependent effective interactions, engineered to promote nematicity. While it ties metamagnetism and nematicity in an ingenious way, it still leaves open the issue of the possible microscopic origins of such phenomena. In particular, it does not address the issue of what features of the material's electronic structure are most important in accounting for its phase diagram.

Here, we address this issue by considering a more realistic model of the electronic structure of $Sr_3Ru_2O_7$. Since both band-structure calculations and angle-resolved photoemission (ARPES) experiments show that there are at least three bands at the Fermi energy per Ru atom (six per bilayer), we consider a model (Sec. I) with three Wannier functions, corresponding loosely to the Ru d_{xz}, d_{yz}, and d_{xy} orbitals (Fig. 2). The former two give rise (as we discuss in Sec. II) to

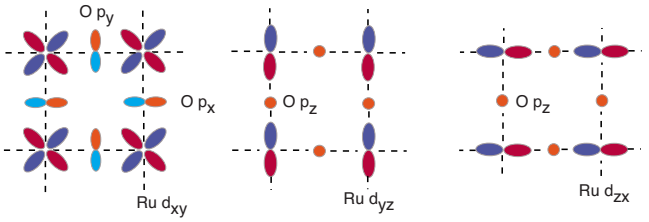

FIG. 2. (Color online) The Ru d_{xy}, d_{yz}, d_{xz} orbitals in a single layer of $Sr_3Ru_2O_7$ in the *ab* plane. π overlaps between two like orbitals along nearest-neighbor bonds are mediated by the intervening oxygen *p* orbitals. For two identical d_{ij} orbitals ($i \neq j$ and $i,j = x,y,z$), the hopping along the $\hat{i}$ direction is strong and is mediated by the oxygen p_j orbital and vice versa. δ overlaps between two identical *d* orbitals along a nearest-neighbor bond do not make use of the oxygens and are therefore much weaker in comparison. Furthermore, all nearest-neighbor hopping between two distinct *d* orbitals vanish by symmetry.

crisscrossing quasi-one-dimensional (1D) bands while the latter gives rise to quasi-2D bands. Each of these bands is, moreover, split in two by the interbilayer hopping, which is substantial in the case of the quasi-1D bands. The multiorbital band structure also implies the existence of an on-site spin-orbit coupling of moderate strength. We study the ordered phases produced by physically reasonable local (on-site) Coulomb interactions using unrestricted Hartree-Fock wave functions (see Fig. 4).

In the multiband context, the nematic phase corresponds to a particular *orbital-ordered* broken-symmetry configuration. Moreover, we will show below that transitions into such a nematic phase are naturally accompanied by metamagnetic transitions. Because the 1D bands are closer to the vH points and because of the stronger divergence of the density of states, ν, at the vH point in 1D, ($\nu \sim 1/\sqrt{E}$), we find that both nematicity and metamagnetism order are primarily driven by a collective reordering of these bands. In addition, a number of other qualitative features of the experimentally observed phase diagram occur naturally and generically from the mean-field solution of the present model:

(1) The interval in which the nematic phase occurs can be tuned to be relatively small $(H_{c2}-H_{c1})/H_{c2} \ll 1$. (See Fig. 6.)

(2) There is an asymmetry to the problem, apparent in Fig. 6 and in the experimental data, which results in a monotonic decrease in the nematic order as H rises from H_{c1} to H_{c2}, resulting in a smaller change in the nematicity at H_{c2} than at H_{c1}. This feature arises in our model due to the underlying asymmetry in the electronic density of states near the vH singularity of the quasi-1D bands.

(3) Our model naturally accounts for why metamagnetism and nematic phases do not occur in the monolayer ruthenate Sr_2RuO_4. The strong bilayer splitting in $Sr_3Ru_2O_7$ places the Fermi level in a region where the density of states of the 1D bands has pronounced positive curvature, satisfying the requirement of the Landau theory of a weakly first-order metamagnetic transition.[19]

(4) Even a moderate spin-orbit coupling, $\lambda_{so} \sim 0.2t$, consistent with band structure estimates,[20,21] produces an order 1 decrease in the critical fields as θ varies from 0° to 90°. (See Fig. 9.)

(5) The near-perfect nesting of the quasi-1D bands accounts for the most prominent peaks in the low-energy magnetic-structure factor observed in neutron-scattering experiments at $H=0$.[22,23] However, the spin-orbit coupling is remarkably efficient at spoiling this nesting, thus plausibly explaining why spin-density-wave (SDW) order does not actually materialize (at least for $H=0$).[22,23]

Clearly, there are many aspects of the physics that are more subtle and cannot be addressed, even qualitatively, at mean-field level. There is, after all, considerable evidence of the effects of strong quantum fluctuations associated with the narrowly pre-empted metamagnetic quantum critical point. We will return to these shortcomings at the end of the paper.

II. MODEL

We have studied a simple tight-binding model of a single RuO_4 bilayer with terms organized according to a hierarchy of scales,

$$H = H_1 + H_{so} + H_2 + \cdots, \tag{1}$$

where H_1 contains the largest terms, which involve the most direct π overlaps between Ru d orbitals on nearest-neighbor sites: the largest hoppings between two neighboring identical $d_{\alpha\alpha'}$ orbitals $(\alpha,\alpha'=x,y,z,\alpha\neq\alpha')$ are along the crystalline $\hat{\alpha}$ and $\hat{\alpha}'$ directions. These hoppings in turn make use of the intervening oxygen p orbitals. The single bilayer approximation is a good one because transport measurements confirm the existence of highly two-dimensional transport and therefore weak bilayer-bilayer coupling. H_1 also includes the on-site Coulomb repulsion terms between two electrons on the same orbital (U) as well as between two electrons in different orbitals (V). H_{so} captures the effect of on-site spin-orbit coupling. H_2 represents the kinetic-energy terms due to weaker δ overlaps between the orbitals (e.g., along the $\hat{z}$ direction for the d_{xy} orbitals). Still smaller terms, some of which we will mention below, are represented by the ellipsis.

Let $d^{\dagger}_{\alpha,\sigma,\vec{R},\lambda}$ create an electron with spin polarization σ at horizontal position $\vec{R}$, in layer $\lambda=\pm1$, and in orbital $\alpha=x,y,z$ corresponding to the d_{xz}, d_{yz}, or d_{xy} orbital, respectively. In order to emphasize the underlying symmetries of the Hamiltonian, we define a spinor field

$$\Psi^{\dagger}_{\alpha\sigma}(\vec{R},\lambda) = d^{\dagger}_{\alpha,\sigma,\vec{R},\lambda}, \quad \alpha = x,y,z. \tag{2}$$

In terms of these and $n_{\lambda,\alpha,\vec{R}}=\Sigma_\sigma d^{\dagger}_{\alpha,\sigma,\vec{R},\lambda}d_{\alpha,\sigma,\vec{R},\lambda}$,

$$\begin{aligned} H_1 = &-t\sum_{\lambda,\vec{R}}\Big[\Psi^{\dagger}(\vec{R},\lambda)(\hat{T}^x+\hat{T}^z)\Psi(\vec{R}+\hat{x},\lambda)+\Psi^{\dagger}(\vec{R},\lambda)(\hat{T}^y \\ &+\hat{T}^z)\Psi(\vec{R}+\hat{y},\lambda)+\frac{1}{2}\Psi^{\dagger}(\vec{R},-\lambda)(\hat{T}^x+\hat{T}^y)\Psi(\vec{R},\lambda) \\ &+\text{H.c.}\Big]+\frac{U}{2}\sum_{\lambda,\alpha,\vec{R}}n^2_{\lambda,\alpha,\vec{R}}+\frac{V}{2}\sum_{\lambda,\alpha\neq\alpha'\vec{R}}n_{\lambda,\alpha,\vec{R}}n_{\lambda,\alpha',\vec{R}} \\ &-\vec{H}\cdot\sum_{\vec{R},\lambda}\Psi^{\dagger}(\vec{R},\lambda)(\vec{L}+\vec{S})\Psi(\vec{R},\lambda). \end{aligned} \tag{3}$$

The contraction over the spinor subscript indices is implied, and we have defined the following matrices:

$$\begin{aligned} \hat{T}^i_{\alpha\beta;\sigma\sigma'} &= \delta_{\alpha\beta}\delta^i_{\alpha}\delta_{\sigma\sigma'}, \\ L^i_{\alpha\beta;\sigma\sigma'} &= \ell^i_{\alpha\beta}\delta_{\sigma\sigma'}, \\ S^i_{\alpha\beta;\sigma\sigma'} &= \delta_{\alpha\beta}\tau^i_{\sigma\sigma'}, \end{aligned} \tag{4}$$

where $\vec{\ell}$ are the orbital angular momenta projected onto the t_{2g} states (an explicit form of these are given in Sec. III) and $\vec{\tau}$ are the Pauli matrices. The final term above is the Zeeman coupling to an external field. We note that in the t_{2g} subspace, the angular momentum is only partially quenched since it is possible, for example, to form linear combinations of orbitals $d_{xz}\pm id_{yz}$ which are eigenstates of ℓ^z. Therefore, the external magnetic field will couple both to $\vec{L}$ and $\vec{S}$.

The on-site spin-orbit coupling Hamiltonian is

$$H_{so} = \lambda_{so}\sum_{\vec{R},\lambda}\Psi^{\dagger}(\vec{R},\lambda)(\vec{L}\cdot\vec{S})\Psi(\vec{R},\lambda), \tag{5}$$

and the smaller nearest-neighbor couplings are

$$\begin{aligned} H_2 = &-t'\sum_{\vec{R},\lambda}\Big[\Psi^{\dagger}(\vec{R},\lambda)\hat{T}^x\Psi(\vec{R}+\hat{y},\lambda)+\Psi^{\dagger}(\vec{R},\lambda)\hat{T}^y\Psi(\vec{R}+\hat{x},\lambda) \\ &+\frac{1}{2}\Psi^{\dagger}(\vec{R},\lambda)\hat{T}^z\Psi(\vec{R},-\lambda)+\text{H.c.}\Big]. \end{aligned} \tag{6}$$

So far, in writing the above terms, we have assumed locally perfect octahedral symmetry with the result, for example, that the hopping matrix element, t, between d_{xz} orbitals on sites separated by one lattice constant in the x direction or on equivalent sites in neighboring planes of a bilayer are equal to each other. The actual material deviates slightly from this ideal symmetry;[24] small terms that break this symmetry as well as further range-hopping terms and interactions are all represented schematically by the ellipsis in Eq. (1) and will not be considered explicitly here.

The Fermi surface of our model taking into account the kinetic terms of H_1, H_2 and also the spin-orbit term H_{so} is shown in Fig. 3(a). It is useful to contemplate its relation to the simpler Fermi surface [shown in Fig. 3(b)] obtained by setting the couplings in H_2 and H_{so} to 0. In this simpler model, hoppings only along the strongest bonds of each orbital are taken into account and consequently, there are perfect one-dimensional bands which are split by the bilayer hopping and form the straight patches of the Fermi surface. These Fermi sheets are purely d_{xz}, d_{yz} in orbital character. Moreover, the 2D bands which come from the d_{xy} orbital are degenerate at this level of approximation. Were we to include the effects of the smaller hopping terms in H_2, a small splitting of the 2D bands and a slight warping of the 1D bands would result; but there still would not be any mixing between bands, and hence there would be multiple points at which two pieces of the Fermi surface would cross one another. When spin-orbit coupling is included, these degeneracies are lifted as is evident from Fig. 3(a). Therefore, H_{so} has the important qualitative effect of changing the Fermi-

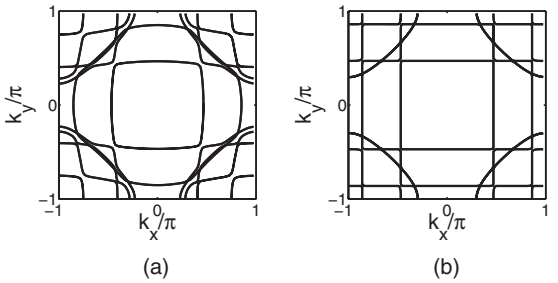

FIG. 3. (a) A "realistic" tight-binding Fermi surface of $Sr_3Ru_2O_7$ taking into account the kinetic energy terms in H_1, H_2 as well as H_{so}. Here, $t'=0.1t$ and $\lambda_{so}=0.2t$. (b) Fermi surface derived from an idealized model taking into account only the single-particle terms in H_1. In the nematic phase, one of the "spin-up" bonding bands crosses the vH point at either $(\pi,0)$ or $(0,\pi)$ depending on the sign of the nematic order parameter (to be defined below). Quotes are placed around spin-up because in the presence of spin-orbit coupling, the magnetic field lifts the degeneracy of Kramers' doublets, and in this case, it is the appropriate pseudospin band which crosses the vH point.

surface topology even if its magnitude is small. We will study the consequences of including H_{so} in Sec. III.

The d_{xy} bands play little active role in the physics discussed below, so we will for the most part ignore these bands altogether, treating them instead simply as a particle reservoir which allows us to perform calculations involving the remaining bands at constant chemical potential rather than at constant density.

III. MEAN-FIELD THEORY

We first consider an idealized model of a bilayer consisting of two orbitals (d_{xz},d_{yz}) in each layer. For the moment, we neglect the curvature of the Fermi surface and any mixing between the two orbitals. In this limit, the orbitals form perfect one-dimensional bands that are bilayer split due to the hopping along the c axis. In the presence of these multiple orbital degrees of freedom, it is natural to consider spin and orbital-ordered broken-symmetry states and so we define the following sets of collective variables:

$$N_\lambda = \sum_{\vec{R}} \langle \Psi^\dagger(\vec{R},\lambda)(\hat{T}^x + \hat{T}^y)\Psi(\vec{R},\lambda)\rangle,$$

$$\vec{M}_\lambda = \sum_{\vec{R}} \langle \Psi^\dagger(\vec{R},\lambda)[\vec{S}(\hat{T}^x + \hat{T}^y)]\Psi(\vec{R},\lambda)\rangle,$$

$$N^o_\lambda = \sum_{\vec{R}} \langle \Psi^\dagger(\vec{R},\lambda)(\hat{T}^x - \hat{T}^y)\Psi(\vec{R},\lambda)\rangle,$$

$$\vec{N}^s_\lambda = \sum_{\vec{R}} \langle \Psi^\dagger(\vec{R},\lambda)[\vec{S}(\hat{T}^x - \hat{T}^y)]\Psi(\vec{R},\lambda)\rangle. \quad (7)$$

These represent, respectively, the total electron density of the one-dimensional bands, N, their overall magnetization, $\vec{M}$, and the nematic order parameter, N^o, that represents the difference in charge density in the two bands, and lastly, we also define $\vec{N}^s$, which represents the difference in moment in each band. We call this latter quantity the order parameter for the "nematic-spin-nematic" phase.[25] Whereas $\vec{M}$ breaks time reversal (T) and SU(2) symmetry, and N^o breaks the lattice C_4 rotation symmetry (R), the nematic-spin-nematic order breaks SU(2), (T), and (R); however, the product (TR) is not broken in this phase. In the presence of an externally applied magnetic field, there is no distinction between the nematic and the nematic-spin-nematic phases.

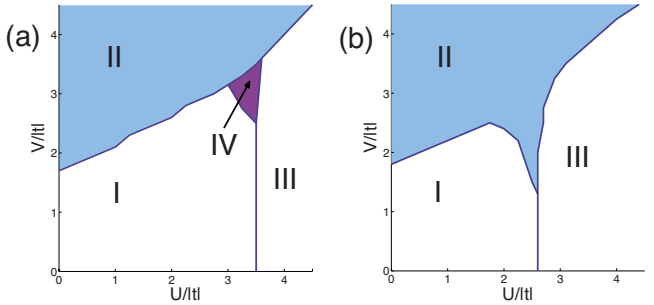

FIG. 4. (Color online) Mean-field $T=0$ phase diagram in the U-V plane in the absence of spin-orbit coupling for $\mu=0.81$ (a) at zero applied field and (b) in finite field, taken here to be $|\vec{H}|=0.04t$. In zero field (a), there are four distinct phases: a paramagnetic region (i), a nematic region (shown in blue) (II), a region in which the ferromagnet and nematic-spin-nematic phases are degenerate but do not coexist (III), and a region in which the nematic, ferromagnet, and nematic-spin-nematic phases coexist (purple region) (IV). All phase boundaries correspond to first-order transitions. In a finite field (b), all regions acquire a nonzero magnetic moment. Regions I and III do not have nematic order, whereas region II contains nematic order. In this case, phase boundaries correspond to metamagnetic transitions. For $U \approx V$ chosen such that at zero field, the parameters lie in region I in (a) above, a field sweep moves the phase boundaries closer to the origin so that the system traverses regions $I \rightarrow II \rightarrow III$ in (b) as the field increases. In this way, the system exhibits a nematic phase precisely between two metamagnetic transitions.

The mean-field phase diagram of our model is presented in Fig. 4. The details of the calculations are presented in the Appendix. The zero-field phase diagram (a) consists of four phases: (I) a paramagnetic phase, (II) a nematic phase, (III) a phase in which the ferromagnet and nematic-spin-nematic are degenerate but do not coexist, and (IV) a coexistence phase of nematic, nematic-spin-nematic, and ferromagnetism. All phase boundaries shown here are first-order transitions. When the magnetic field is nonzero (b), the ferromagnetic phase has a lower free energy than the nematic-spin-nematic phase and this degeneracy is lifted.

In a nonzero field, all phase boundaries become metamagnetic transitions. Two qualitatively different features arise in this case. First, there are only two types of phases: either magnetic order is present alone (I and III) or magnetic order coexists with nematic order (II). In (b), the only difference between regions I and III is the size of the moment (larger in region III). Note, in particular, that with increasing magnetic field, phase III moves in to smaller values of U and V. Thus, without requiring any fine tuning, it is possible for the sys-

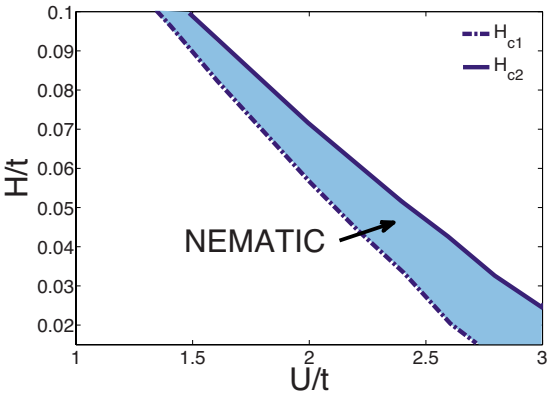

FIG. 5. (Color online) Phase diagram at zero temperature in the U-H plane with $U=V$ in the absence of spin-orbit coupling for $\mu=0.81$. For each $U=V$, as the field is increased, two metamagnetic transitions occur and are denoted H_{c1} (dashed line) and H_{c2} (solid line). For $H_{c1}<H<H_{c2}$ a nematic phase (blue region) occurs, corresponds to region II in Fig. 4(b), and collapses onto region IV in Fig. 4(a) in the zero-field limit. Although we have chosen $U=V$ in this figure, we emphasize that a phase diagram with the same topology occurs if we set $U=\alpha V$, for a range of α, so long as the line $U=\alpha V$ crosses each of the three regions shown in Fig. 4(b).

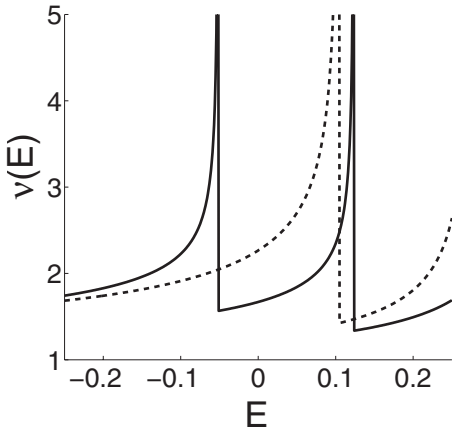

FIG. 7. Single quasiparticle density of states (arbitrary units) in the nematic phase, $H=0.04t, U=V=2.5t, \mu=0.81t$. The Fermi energy is at $E=0$. The dashed line corresponds to the quasiparticle density of states at $H=0.02t$, there the nematic phase does not arise. Since the nematic phase has a lower density of states, it is expected that in mean-field theory, it will also have a lower entropy at temperatures small compared to μ.

tem studied here to undergo a sequence of metamagnetic transitions, starting with a paramagnetic phase and ending with a ferromagnetic phase with nematic order sandwiched in between as shown in Fig. 5. The requirements for such a phenomenon to occur in our model is that $U \approx V$. For $U \gg V$, for instance, the effect of applying a magnetic field is to induce ferromagnetism alone. By contrast, when $U \approx V$, this ferromagnetic phase is pre-empted at low fields by a nematic phase. Figure 6 shows the magnetization and nematic order as a function of field for a particular value of $U=V=2.5t$. Here it is clearly seen that as the field sweeps across the first metamagnetic transition, nematic order develops; when the field is increased further, a second metamagnetic transition occurs which destroys the nematic phase.

In Fig. 7, the single quasiparticle density of states is plotted in the nematic phase. There is a double peak near the Fermi level whose splitting corresponds to the size of the nematic gap. Also shown in Fig. 7 is the density of states at a slightly lower field where the system is just about to enter the nematic phase. We note that there is a reduction in the quasiparticle density of states at the Fermi level in the nematic phase; this in turn implies that the entropy of the nematic phase at low temperatures within mean-field theory is lower than the neighboring isotropic phases. This is also seen in Fig. 8 from the curvature of the phase boundaries of the nematic phase at finite temperatures. We highlight here that this result from mean-field theory disagrees with the experimental observations reported in Ref. 12 where the nematic phase boundaries "fan" outward, implying that in actuality, the nematic phase has a higher entropy than the neighboring isotropic phases. We believe that this effect must stem from fluctuations (both thermal and quantum) due to the presence of nematic domains.

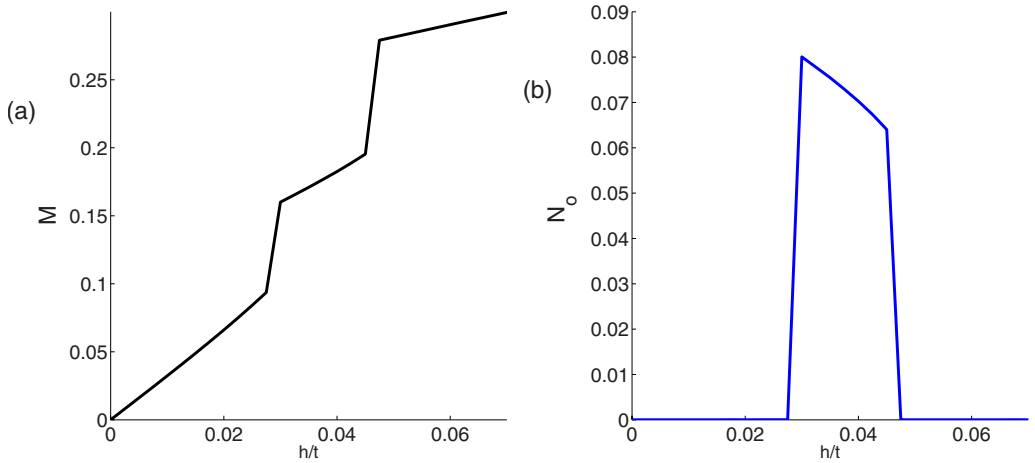

FIG. 6. (Color online) (a) Magnetization and (b) nematicity as a function of applied field for $U=V=2.5t$ and $\mu=0.81t$ in the absence of spin-orbit coupling. The nematic phase is found to lie precisely between the two metamagnetic transitions.

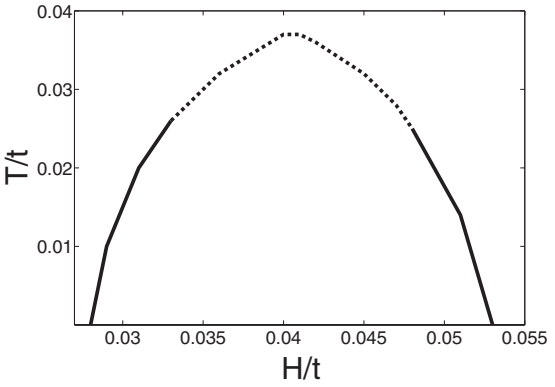

FIG. 8. Phase diagram of the system without spin-orbit coupling showing the finite temperature boundaries of the nematic phase. First-order transitions (solid curve) at low temperatures give way to continuous transitions (dashed curve) at higher temperatures as the vH singularities get smoothed out. Finite temperature metamagnetic crossovers away from the nematic phase are not shown. Here, $U=V=2.5t$, $\mu=0.81t$, and $\lambda=0.2t$.

IV. EFFECT OF SPIN-ORBIT COUPLING: ANGLE-DEPENDENT METANEMATIC TRANSITIONS

The results above were based on the assumption that spin SU(2) symmetry is preserved in the system. However, the experimental phase diagram[6] of $Sr_3Ru_2O_7$ (Fig. 1) exhibits an $O(1)$ anisotropy in the critical field at which a metamagnetism occurs: the critical field with H along the c axis is about 1.6 times larger than the case when it points in the ab plane. A natural way to account for this anisotropy is to consider the effect of spin-orbit coupling in the material. Since the material has an inversion center, k-dependent spin-orbit interactions, such as the Rashba coupling, are forbidden, and we proceed by considering the effect of an atomic spin-orbit coupling, given in Eq. (5). While the precise magnitude of the spin-orbit coupling constant λ_{so} for this material is unclear, local-density approximation (LDA) calculations of the monolayer ruthenate compound Sr_2RuO_4 suggest that λ_{so} is approximately 10% of E_f.[20,21] Indeed, in recent ARPES studies of $Sr_3Ru_2O_7$, LDA calculations had to employ spin-orbit coupling in order to fit properly to the Fermi surface.[26] Since this spin-orbit coupling term is onsite, it seems reasonable to expect that similar values also hold for the bilayer compound.

When such spin-orbit coupling terms are included in the Hamiltonian, the d_{xy} band must necessarily be taken into account. However, since the spin-orbit coupling is smaller than the crystal-field splitting, we can treat it as a perturbation and project the angular momentum operator $\boldsymbol{L}$ onto the t_{2g} subspace. To be more explicit, a valid choice of the orbital angular momentum operators projected onto the t_{2g} manifold is

$$\ell^x = \begin{pmatrix} 0 & 0 & 0 \\ 0 & 0 & -1 \\ 0 & -1 & 0 \end{pmatrix}, \quad \ell^y = \begin{pmatrix} 0 & 0 & -1 \\ 0 & 0 & 0 \\ -1 & 0 & 0 \end{pmatrix},$$

$$\ell^z = -i[\ell^x, \ell^y]. \tag{8}$$

In terms of these operators, the spin-orbit coupling in each layer of our system is represented by the 6×6 matrix,

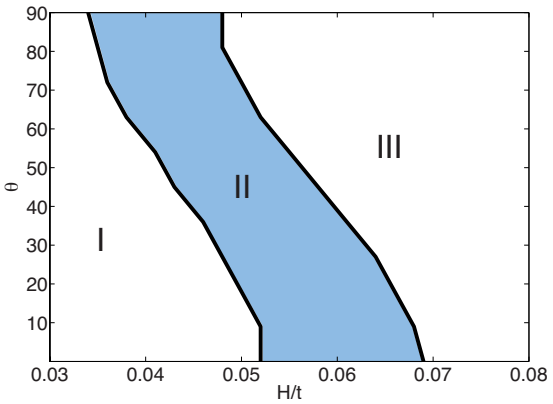

FIG. 9. (Color online) Angle-dependent metanematic phase boundaries in the presence of spin-orbit coupling showing an $O(1)$ anisotropy in the critical fields. When the field is tilted toward the ab plane, the C_4 point-group symmetry is automatically broken. In region I at low fields, the moment is small and there is also a small nematic phase present for all $\theta>0$. The first metamagnetic transition into region II gives rise to an accompanying jump in nematicity in addition to the magnetization. Finally, the second metamagnetic transition into region III results in a discontinuous decrease in the size of the nematic order parameter as well as a jump in magnetization. Here, $U=V=2.5t$, $\mu=0.81t$, and $\lambda_{so}=0.2t$.

$$\boldsymbol{L}\cdot\boldsymbol{S} = \begin{pmatrix} \ell^z & \ell^x - i\ell^y \\ \ell^x + i\ell^y & -\ell^z \end{pmatrix}. \tag{9}$$

Having in mind the framework of a minimal model which captures the essential features of the experimental phase diagram, we first treat the quasi-2D band as a free-electron system and neglect the effect of Coulomb interactions. We have checked that the inclusion of a Hubbard repulsion on this band produces no qualitative changes to the results reported here. Furthermore, we neglect the terms in H_2 as before. This way, the mean-field order parameters in the presence of spin-orbit coupling are identical to those in Eq. (7), and the spin-quantization axis is defined to be in the direction of the applied field. However, the spin-orbit coupling term is sensitive to the orientation of the magnetic field relative to the c axis since the orbital angular momentum operators above are defined with respect to the crystalline axis of the system. More explicitly, in the tilted field, the spin-orbit term is modified as

$$H_{so}(\theta) = \lambda_{so}\boldsymbol{L}\cdot\tilde{\boldsymbol{S}}(\theta),$$

$$\tilde{\boldsymbol{S}}(\theta) = \exp\left(-i\frac{\vec{\sigma}\cdot\vec{n}}{2}\theta\right)\boldsymbol{S}\exp\left(i\frac{\vec{\sigma}\cdot\vec{n}}{2}\theta\right), \tag{10}$$

where θ is the angle of the applied field relative to the c axis and $\vec{n}$ is a unit vector either in the crystalline a or b direction.

In Fig. 9, we show the phase diagram in the H-θ plane, keeping $U=V$ fixed and $\lambda_{so}=0.2t$. As the field is tilted toward the ab plane, we see that the critical field at which the metamagnetic transition occurs is smaller in magnitude. For all angles, there are two metamagnetic transitions with a nematic phase in between. When the field is tilted away from the c axis, the crystalline C_4 symmetry is broken, and we distinguish a phase in which the nematic order jumps from a small

value (region I) to a large value (region II) and jumps back to a small value (region III). Thus the tilted field shows the nematic analog of metamagnetic transitions, and we refer to these transitions here as "metanematic" transitions.[27] We note that although we find metamagnetic transitions with the same general angle dependence as seen in experiments, the nematic phase in our model does not have the correct topology in the field-angle plane (compare Figs. 1 and 9). Instead, we find that if a nematic phase occurs, it remains present for all field orientations. Given the structure of the phases shown in Fig. 4(b), it does not appear impossible that the correct topology could emerge under appropriate circumstances; but in the present model, this would require angle-dependent interactions. While such terms are unphysical at the bare microscopic level, they could arise at the effective level due to fluctuation effects that have not been considered here.

The ordering tendencies which we have considered so far do not break lattice translational symmetry. However, inelastic neutron-scattering experiments[22,23] have provided evidence that there are substantial incommensurate spin fluctuations in this system although static SDW order has not been observed at zero external field. The incommensurate spin fluctuations in this system occur primarily due to the partial nesting of the Fermi surface. Therefore, we must check whether such finite $\boldsymbol{q}$ ordering tendencies in this material are favored over the uniform nematic order proposed in this paper. To do this, we have computed the generalized one-loop spin susceptibility

$$[\chi^{ij}(\boldsymbol{q})]^{st}_{ba} = \int_0^\beta d\tau \sum_{\boldsymbol{p}\boldsymbol{p}'} \sum_{\alpha\beta\gamma\delta} \sigma^i_{\alpha\beta}\sigma^j_{\gamma\delta} \times \langle T_\tau d^\dagger_{s\boldsymbol{p}\alpha}(\tau) d_{t\boldsymbol{p}+\boldsymbol{q}\beta}(\tau) d^\dagger_{a\boldsymbol{p}'\gamma}(0) d_{b\boldsymbol{p}'-\boldsymbol{q}\delta}(0)\rangle \tag{11}$$

in the presence of spin-orbit coupling and magnetic field. The electron Hamiltonian is a 12×12 matrix and the electron propagators are spin and orbital dependent which in turn makes the above spin susceptibility a 36×36 matrix. Using the random-phase approximation (RPA), we find that an instability toward the formation of SDW order occurs in the system (taking $U=V$) when U exceeds a critical strength $U_{c,\mathrm{SDW}}$ which satisfies

$$\frac{U_{c,\mathrm{SDW}}}{2}\max(\mathrm{eig}[\chi]) = 1 \tag{12}$$

and for the band-structure parameters we have been using $(\lambda_{so}=0.2t, t'=0, \mu=0.81t)$ the maximal eigenvalue of the susceptibility matrix is obtained at the wave vector $\boldsymbol{q}=(0.27,0.27)\pi$ where the spin susceptibility $\chi^{zz}(\boldsymbol{q})$ obtains its largest value. From this mean-field estimation, we find that $U_{c,\mathrm{SDW}}\approx 3.1t$, which is also close to the critical coupling required for ferromagnetism, as seen in Fig. 4.

Thus, in addition to accounting for the angle-dependent metamagnetic transitions observed in this system, the inclusion of spin-orbit coupling also naturally explains why static incommensurate SDW order does not occur despite the presence of incommensurate spin fluctuations in this system.

V. DISCUSSION

We have shown in this paper that the remarkable low-temperature properties of $Sr_3Ru_2O_7$ can be understood as being a consequence of orbital ordering of the quasi-1D bands. We have been able to account for most of the gross features of the experiments from a simple microscopic model. Our results are based on a mean-field solution of a system with strong electron interactions and a justification for focusing solely on this approach has not been provided. Although metamagnetism and nematicity generally arise as strong-coupling effects in metals and are therefore difficult to treat in a controlled theoretical fashion, the divergence of the density of states ν at the vH point ensures that the Stoner criterion can be satisfied even for weak interactions, which are much less than the bandwidth. Thus, by the notion of adiabatic continuity, it may be legitimate to treat this problem from a weak-coupling standpoint.

Previous attempts to explain metamagnetism and nematicity in this system[18,28,29] were based on the assumption that the quasi-2D bands drive the nematic and metamagnetic transitions. By contrast, we point out here that it is much more natural to think instead that the quasi-1D bands are responsible for the transitions. We note, from a symmetry standpoint, that the quasi-1D bands form a twofold representation of the C_4 rotation symmetry of this system: thus, the nematic phase which breaks C_4 rotation symmetry corresponds to an orbital ordering among these bands. Furthermore, it is known from experiment that the monolayer ruthenate Sr_2RuO_4 does not exhibit metamagnetism for magnetic fields up to 30 T. The primary difference in the electronic structure of the monolayer vs the bilayer compound is the large bilayer splitting in the latter. We have shown here that while the quasi-2D bands are only weakly affected by the bilayer splitting, the quasi-1D bands are rather strongly affected by it. Thus, the experimental differences between the monolayer and bilayer ruthenate compounds as well as symmetry considerations lead us to propose that quasi-1D bands in this system are primarily responsible for the rich phase diagram of the bilayer ruthenate. Although we propose a different microscopic origin for the Fermi-surface distortion from that used in previous work on the subject, we note that our picture is still one of a weak-coupling Pomeranchuk type. As such it automatically retains the attractive feature, common to any weak anisotropic distortion of electronic structure in the vicinity of E_F, that it naturally predicts a sensitivity to impurity scattering.[30] This in turn matches one of the key experimentally determined characteristics of the behavior that we set out to explain.

Along with the focus on the 1D bands comes the existence of a nesting vector, $2k_F$, and the issue of SDW order. At mean-field level, the preferred SDW instability for a pair of orthogonal quasi-1D bands leads[31] either to bidirectional order with ordering vectors $(2k_F,\pi)$ and $(\pi,2k_F)$ or unidirectional order with ordering vector $(2k_F,2k_F)$. However, inelastic neutron-scattering studies have found that the most dominant peaks are observed in the $(2k_F,0)$ direction.[22] Nevertheless, we have shown that even moderate spin-orbit coupling reduces the nesting to the extent that the *mean-field* tendency to nematic and SDW ordering are comparably

strong. Moreover, we expect fluctuation effects to reduce the ordering tendency of an incommensurate SDW (which has a gapless sliding mode and two nearly gapless spin-wave modes) relative to the Ising-type nematic order, especially given the quasi-2D structure of this material, which makes fluctuational corrections all the more significant.

However, there are still two qualitatively important features of the experimental data that are not well accounted for by any mean-field treatment we know of: (1) the intermediate nematic phase has been shown, in experiment, to have higher entropy at low temperatures than either of the adjacent disordered phases. In contrast, at mean-field level, the ordered phase always has a lower Fermi-surface density of states than the proximate disordered phases and so has smaller low-temperature entropy. (2) Doping studies suggest that at least part of the peaks in the density of states that are thought to drive the metamagnetism are somehow locked to the Fermi energy rather than being purely features of an underlying rigid-band structure. These features we believe are signatures of strong-coupling effects and can be accounted for by a more sophisticated theory in which local nematic order is present over a broad range of magnetic fields (including $B=0$) but only propagates to long distances in the narrow range of B in which macroscopic anisotropies are observed.

More generally, it is clear that fluctuation effects play a significant role in the physics. Even though the putative metamagnetic quantum critical point is pre-empted by the nematic phase, the observed fluctuational phenomena that lead to the conjectured critical point in the first place remain real and dramatic. It is likely that they reflect the existence of a "nearby" quantum critical point, even if it is not actually observed. In this context, mean-field results, of the sort discussed in the present paper, should be adopted with caution. At the very least, the effective parameters that enter our model must be reinterpreted as strongly renormalized effective parameters, given that the observed bandwidths[32] are narrower by a factor of order 10–100 than the bandwidths found in LDA calculations.[33] We defer the fascinating study of fluctuation effects to a future publication.

Finally, we make a comment about the observed resistivity anisotropy in this material when $H\|c$. While we have presented a symmetry argument for why such a resistivity anisotropy ought to be present, we have not explicitly computed the resistivity anisotropy from our model. Indeed, any small nematic Fermi-surface distortion such as that discussed here is unlikely to produce a large effect on the low-temperature resistivity due to the distortion alone. The reason for this is that the nematic phase arises from a discrepancy in electrons which are close to a vH singularity; these, in turn, have a very small characteristic velocity and hence would contribute most weakly to transport signatures. The distortion of the Fermi surface is more likely to change the transport properties by being a source of domains and domain-wall scattering, something which is beyond the scope of the calculations that we report. We note further that in the experiments of Ref. 12 when the field is tilted toward the *ab* plane both the average resistivity and the anisotropy rapidly decrease with angle. In our picture, we imagine that as the field is tilted, nematic domains get aligned and scattering is therefore considerably reduced. Thus, ironically, precisely the same signal which was used to detect the nematic fluid would prove to be useless deep in the nematic phase, when the system forms a single macroscopic nematic order. A more quantitative theory of the physics discussed here will be presented elsewhere.

Note added. As we were preparing to submit this paper, we became aware of a related study by Lee and Wu.[34]

ACKNOWLEDGMENTS

We are grateful to M. Allan, J. C. Davis, E. Fradkin, H.-Y. Kee, R. B. Laughlin, M. Lawler, Y. Maeno, V. Oganesyan, A. Rost, D. J. Scalapino, K. Shen, D. Singh, and H. Yao for insightful discussions. This work was supported in part by the Cornell Center for Materials Research through NSF under Grant No. 0520404 (E.A.K.), the Sloan Foundation, NSERC and the Ontario ERA (A.P.), NSF under Grant No. DMR 0758356 (S.A.K.), and the Stanford Institute for Theoretical Physics (S.R.).

APPENDIX: METAMAGNETISM AND NEMATICITY OF QUASI-1D BANDS

Here, we present, for the sake of clarity, the derivation of the mean-field equations which were used to deduce the phase diagram in Fig. 4. The mean-field order parameters are defined via

$$\langle n_{x,\lambda,\vec{R},\sigma}\rangle = \frac{1}{4}(N^{\lambda} + N_o^{\lambda} + \sigma M^{\lambda} + \sigma N_s^{\lambda}),$$

$$\langle n_{y,\lambda.\vec{R},\sigma}\rangle = \frac{1}{4}(N^{\lambda} - N_o^{\lambda} + \sigma M^{\lambda} - \sigma N_s^{\lambda}). \tag{A1}$$

After decomposing the interactions in terms of the above expectation values, we arrive at the following one-particle Hamiltonian:

$$H(\vec{k}) = \begin{pmatrix} H_x(\vec{k}) & 0 \\ 0 & H_y(\vec{k}) \end{pmatrix}, \tag{A2}$$

where

$$H_a(\vec{k}) = -2t\cos k_a\, \hat{1}_{4\times 4} + \begin{pmatrix} \delta\mu_{a,\uparrow}^{(1)} - h & 0 & -t & 0 \\ 0 & \delta\mu_{a,\downarrow}^{(1)} + h & 0 & -t \\ -t & 0 & \delta\mu_{a,\uparrow}^{(-1)} - h & 0 \\ 0 & -t & 0 & \delta\mu_{a,\downarrow}^{(-1)} + h \end{pmatrix}$$

and $a=x,y$. We have also defined the quantities

$$\delta\mu_{x,\sigma}^{(\lambda)} = \frac{U}{4}(N_o^{\lambda} - \sigma M^{\lambda} - \sigma N_s^{\lambda}) - \frac{V}{2}N_o^{\lambda},$$

$$\delta\mu_{y,\sigma}^{(\lambda)} = \frac{U}{4}(-N_o^{\lambda} - \sigma M^{\lambda} + \sigma N_s^{\lambda}) + \frac{V}{2}N_o^{\lambda}. \tag{A3}$$

Thus, by neglecting the hybridization between the x,y orbitals, the mean-field Hamiltonian takes the block-diagonal

form above and the quasiparticle bonding and antibonding energies are easily obtained:

$$\epsilon^{x}_{\pm\sigma} = -2t\cos k_x - \sigma h + \frac{1}{2}(\delta\mu^{(1)}_{x,\sigma} + \delta\mu^{(-1)}_{x,\sigma}) \pm \sqrt{t^2 + \frac{1}{4}(\delta\mu^{(1)}_{x,\sigma} - \delta\mu^{(-1)}_{x,\sigma})^2},$$

$$\epsilon^{y}_{\pm\sigma} = -2t\cos k_y - \sigma h + \frac{1}{2}(\delta\mu^{(1)}_{y,\sigma} + \delta\mu^{(-1)}_{y,\sigma}) \pm \sqrt{t^2 + \frac{1}{4}(\delta\mu^{(1)}_{y,\sigma} - \delta\mu^{(-1)}_{y,\sigma})^2}. \quad \text{(A4)}$$

Due to the 1D band dispersion, it is possible to obtain the density of states and the grand-canonical free-energy density analytically by summing over the eight quasiparticle bands of this model. At zero temperature,

$$F = F_0(M^{\lambda}, N^{\lambda}_s, N^{\lambda}_o) + \int_{-\infty}^{\mu} (E-\mu)\nu(E)dE,$$

$$F_0(M^{\lambda}, N^{\lambda}_s, N^{\lambda}_o) = \frac{U}{8}\sum_{\lambda}[(\bar{N}^{\lambda})^2 + (M^{\lambda})^2 + (N^{\lambda}_s)^2 - (N^{\lambda}_o)^2] + \frac{V}{4}\sum_{\lambda}[(\bar{N}^{\lambda})^2 + (N^{\lambda}_o)^2], \quad \text{(A5)}$$

$$\begin{aligned}\int_{-\infty}^{\mu}(E-\mu)\nu(E)dE = &-\frac{2}{\pi}\mathrm{Re}\sum_{a=x,y}\sum_{\sigma,\sigma'=\pm1}\left[1-\frac{1}{4}\left\{\mu+\sigma h-\frac{1}{2}[\delta\mu^{(1)}_{a,\sigma}+\delta\mu^{(-1)}_{a,\sigma}]+\sigma'\sqrt{t^2+\frac{1}{4}[\delta\mu^{(1)}_{a,\sigma}-\delta\mu^{(-1)}_{a,\sigma}]^2}\right\}^2\right]^{1/2}\\ &-\frac{2}{\pi}\mathrm{Re}\sum_{\sigma,a=x,y}\sum_{\sigma'=\pm1}\frac{1}{2}\left\{\mu+\sigma h-\frac{1}{2}[\delta\mu^{(1)}_{a,\sigma}+\delta\mu^{(-1)}_{a,\sigma}]+\sigma'\sqrt{t^2+\frac{1}{4}[\delta\mu^{(1)}_{a,\sigma}-\delta\mu^{(-1)}_{a,\sigma}]^2}\right\}^2\\ &\times\sin^{-1}\left\{\frac{\mu+\sigma h-\frac{1}{2}[\delta\mu^{(1)}_{a,\sigma}+\delta\mu^{(-1)}_{a,\sigma}]+\sigma'\sqrt{t^2+\frac{1}{4}[\delta\mu^{(1)}_{a,\sigma}-\delta\mu^{(-1)}_{a,\sigma}]^2}}{2}\right\}. \quad \text{(A6)}\end{aligned}$$

The phase diagram is then obtained by minimizing the above free energy with respect to the order parameters. We note that even upon including curvature effects in the band structure, the grand-canonical free-energy density can be expressed analytically in terms of complete elliptic integrals. However, for the sake of simplicity, we do not include such terms here. While such Fermi terms do modify the precise location of phase boundaries, they have no qualitative effect on the physics.

[1] A. P. Mackenzie and Y. Maeno, Rev. Mod. Phys. **75**, 657 (2003).
[2] C. Bergemann, A. P. Mackenzie, S. R. Julian, D. Forsythe, and E. Ohmichi, Adv. Phys. **52**, 639 (2003).
[3] S. G. Ovchinnikov, Phys. Usp. **46**, 21 (2003).
[4] V. J. Emery and S. A. Kivelson, Physica C **235-240**, 189 (1994).
[5] R. S. Perry *et al.*, Phys. Rev. Lett. **86**, 2661 (2001).
[6] S. A. Grigera, R. A. Borzi, A. P. Mackenzie, S. R. Julian, R. S. Perry, and Y. Maeno, Phys. Rev. B **67**, 214427 (2003).
[7] S. A. Grigera, R. S. Perry, A. J. Schofield, M. Chiao, S. R. Julian, G. G. Lonzarich, S. I. Ikeda, Y. Maeno, A. J. Mills, and A. P. Mackenzie, Science **294**, 329 (2001).
[8] A. J. Millis, A. J. Schofield, G. G. Lonzarich, and S. A. Grigera, Phys. Rev. Lett. **88**, 217204 (2002).
[9] R. S. Perry, K. Kitagawa, S. A. Grigera, R. A. Borzi, A. P. Mackenzie, K. Ishida, and Y. Maeno, Phys. Rev. Lett. **92**, 166602 (2004).
[10] S. A. Kivelson, E. Fradkin, and V. J. Emery, Nature (London) **393**, 550 (1998).
[11] V. Oganesyan, S. A. Kivelson, and E. Fradkin, Phys. Rev. B **64**, 195109 (2001).
[12] R. A. Borzi, S. A. Grigera, J. Ferrell, R. S. Perry, S. J. S. Lister, S. L. Lee, D. A. Tenant, Y. Maeno, and A. P. Mackenzie, Science **315**, 214 (2007).
[13] B. Binz and M. Sigrist, Europhys. Lett. **65**, 816 (2004).
[14] S. A. Grigera *et al.*, Science **306**, 1154 (2004).
[15] C. Wu, K. Sun, E. Fradkin, and S.-C. Zhang, Phys. Rev. B **75**, 115103 (2007).
[16] H. Yamase and H. Kohno, J. Phys. Soc. Jpn. **69**, 2151 (2000).
[17] C. J. Halboth and W. Metzner, Phys. Rev. Lett. **85**, 5162 (2000).
[18] H.-Y. Kee and Y. B. Kim, Phys. Rev. B **71**, 184402 (2005).
[19] E. P. Wohlfarth and P. Rhodes, Philos. Mag. **7**, 1817 (1962).
[20] M. W. Haverkort, I. S. Elfimov, L. H. Tjeng, G. A. Sawatzky, and A. Damascelli, Phys. Rev. Lett. **101**, 026406 (2008).
[21] G.-Q. Liu, V. N. Antonov, O. Jepsen, and O. K. Andersen, Phys. Rev. Lett. **101**, 026408 (2008).
[22] L. Capogna, E. M. Forgan, S. M. Hayden, A. Wildes, J. A. Duffy, A. P. Mackenzie, R. S. Perry, S. Ikeda, Y. Maeno, and S. P. Brown, Phys. Rev. B **67**, 012504 (2003).
[23] S. Ramos *et al.*, Physica B **403**, 1270 (2008).
[24] H. Shaked, J. D. Jorgensen, O. Chmaissem, S. Ikeda, and Y. Maeno, J. Solid State Chem. **154**, 361 (2000).
[25] S. A. Kivelson, E. Fradkin, V. Oganesyan, J. M. Tranquada, A.

Kapitulnik, and C. Howald, Rev. Mod. Phys. **75**, 1201 (2003).
[26] A. Tamai, M. P. Allan, J. F. Mercure, W. Meevasana, R. Dunkel, D. H. Lu, R. S. Perry, A. P. Mackenzie, D. J. Singh, Z. X. Shen, and F. Baumberger, Phys. Rev. Lett. **101**, 026407 (2008).
[27] C. Puetter, H. Doh, and H.-Y. Kee, Phys. Rev. B **76**, 235112 (2007).
[28] C. Honerkamp, Phys. Rev. B **72**, 115103 (2005).
[29] A. M. Berridge, A. G. Green, S. A. Grigera, and B. D. Simons, Phys. Rev. Lett. **102**, 136404 (2009).
[30] A. F. Ho and A. J. Schofield, EPL **84**, 27007 (2008).
[31] H. Yao, J. A. Robertson, E.-A. Kim, and S. A. Kivelson, Phys. Rev. B **74**, 245126 (2006).
[32] J. C. Davis (unpublished).
[33] D. J. Singh and I. I. Mazin, Phys. Rev. B **63**, 165101 (2001).
[34] Wei-cheng Lee and Congjun Wu, arXiv:0902.1337 (unpublished).